Imaging the Hydrothermal System of Kirishima Volcanic Complex, Japan with ALOS-1/2 InSAR Time Series

Zhang Yunjun[1,†], Falk Amelung[1], and Yosuke Aoki[2]

[1]Rosentiel School of Marine and Atmospheric Science, University of Miami, Miami, FL, USA.

[2]Earthquake Research Institute, University of Tokyo, Tokyo, Japan.

[†]Now at Seismological Laboratory, California Institute of Technology, Pasadena, CA, USA.

Corresponding author: Z. Yunjun (yunjunzgeo@gmail.com)

Key Points:

- Shinmoe-dake hydrothermal system deflated during the 2008-2010 eruptions, then was replaced by a magmatic body during the 2011 eruption.
- Persistent inflation at the Iwo-yama crater during 2014-2019 is driven by liquid-gas two-phase water boiling.
- Precursory expansion of Iwo-yama's southern and western vent after December 2017 is driven by the upward migration of magmatic fluid.

Abstract

We present deformation measurements of the Kirishima volcanic complex from ALOS-1/2 Interferometric Synthetic Aperture Radar (InSAR) time-series during 2006-2019. Shinmoe-dake deflated ~6 cm during the 2008-2010 phreatic eruptions and inflated ~5 cm prior to the 2017 magmatic eruption. Iwo-yama inflated ~19 cm within the crater since January 2015 and ~7 cm around the southern and western vent since four months before the 2018 eruption. These deformations can be modeled as an ellipsoid at ~700 m depth beneath Shinmoe-dake and as a sphere on top of an ellipsoid at ~130 and ~340 m depths beneath Iwo-yama. Combining geodetic, geoelectric, geochemical and petrological analysis, we interpret the hydrothermal origin of the deflation at Shinmoe-dake and inflation at Iwo-yama; the hydrothermal-magmatic transition during the 2011 Shinmoe-dake eruption; water-boiling and bottom-up pressurization as driving mechanisms of the inflation at Iwo-yama. The study highlights the imaging potential of InSAR time-series on complex hydrothermal systems.

Plain Language Summary

Steam-blast eruptions are driven by the heat of magma interacting with water. Although small in size, they are very common and unpredictable, making them hazardous. In order to know when and where these interactions started and how they led to the eruption, we take the Kirishima volcano group as an example and use 10 years of satellite radar images to measure its ground surface deformation. We find that Shinmoe-dake fell ~6 cm during the 2008-2010 eruptions, much earlier than previously thought; while Iwo-yama rose ~7 cm since four months before its 2018 eruption. Combining models from specialized computer code with previous studies from other disciplines, we explain the fall of Shinmoe-dake and the rise of Iwo-yama are due to the steam release and water accumulation of water-rich zones at ~700 m and ~340 m depth below

the surface, respectively. The water-rich zone of Shinmoe-dake was replaced and filled by magma during the 2011 eruption. These short-lived, small-size deformations have not been identified in the region before, nor has the type of deformation in general been studied extensively worldwide. Future volcano monitoring efforts should take this into account on a regular basis.

1 Introduction

Phreatic eruptions are among the most common but also among the most unpredictable volcanic phenomena, making them hazardous despite the relatively small scale. Unlike magmatic eruptions driven by magma migration, volatile exsolution and crystallization, phreatic eruptions are driven by broadly defined hydrothermal processes, such as interactions among water, rocks and magmatic heat and gas, similar to geyser-like mechanisms but more violent with the expulsion of rocks and mud, usually without juvenile material (Germanovich & Lowell, 1995; Muffler et al., 1971; Stix & Moor, 2018). Many of the largest volcanic eruptions started with phreatic events, e.g. the 1980 Mt. St. Helens eruption (Christiansen et al., 1982) and the 1991 Pinatubo eruption (Newhall & Punongbayan, 1996), but phreatic eruptions may also occur in isolation.

Geophysical monitoring of phreatic eruptions has been challenging due to their localized deformation signals with small magnitude and sudden occurrence with few if any precursors (Kobayashi et al., 2018). Although not as frequently as magmatic processes, ground deformation associated with hydrothermal processes has been observed in all stages of volcanic eruption cycles, including the pre-eruptive (Kobayashi et al., 2018; Narita et al., 2020), co-eruptive (Himematsu et al., 2020), post-eruptive period (Hamling et al., 2016; Nakaboh et al., 2003;

Narita & Murakami, 2018) and non-eruptive unrest period (Battaglia et al., 2006; Lu et al., 2002; Lundgren et al., 2001).

Here we report a decade-long Interferometric Synthetic Aperture Radar (InSAR) deformation time-series of the Kirishima volcanic complex, Japan during 2006-2011 and 2014-2019, covering the 2008 and 2017 Shinmoe-dake eruptions and the 2018 Iwo-yama eruption. We estimate the location, geometry and volume change of the pressure sources and combine them with previous observations from resistivity, geochemistry and petrology to a new model for the shallow plumbing system of the central Kirishima volcanoes.

2 Geological Setting

The Kirishima volcanic complex (Japanese for foggy mountain) is located in southern Kyushu, where the Phillippine Sea Plate is subducted beneath the Amurian Plate (Wallace et al., 2009). The complex consists of more than 25 craters, cones and lava domes produced by the southward migration of eruption centers in the last 330 ka (Fig. 1a; Nakada et al., 2013). These volcanic centers form an elliptical 30 by 20 km northwest-trending zone with younger volcanism generally in the southeast (Chapman et al., 2009). The most active eruptive centers are Iwo-yama (Japanese for sulfur peak), Shinmoe-dake and Ohachi (altitudes of 1,313 m, 1,421 m and 1,408 m, respectively). Hydrothermal systems are widely distributed in shallow levels throughout Kirishima (e.g., Aizawa et al., 2014; Ohba et al., 1997). It has been suggested that the magmatic system beneath connects at depth with Aira caldera located 20 km to the south (Brothelande et al., 2018).

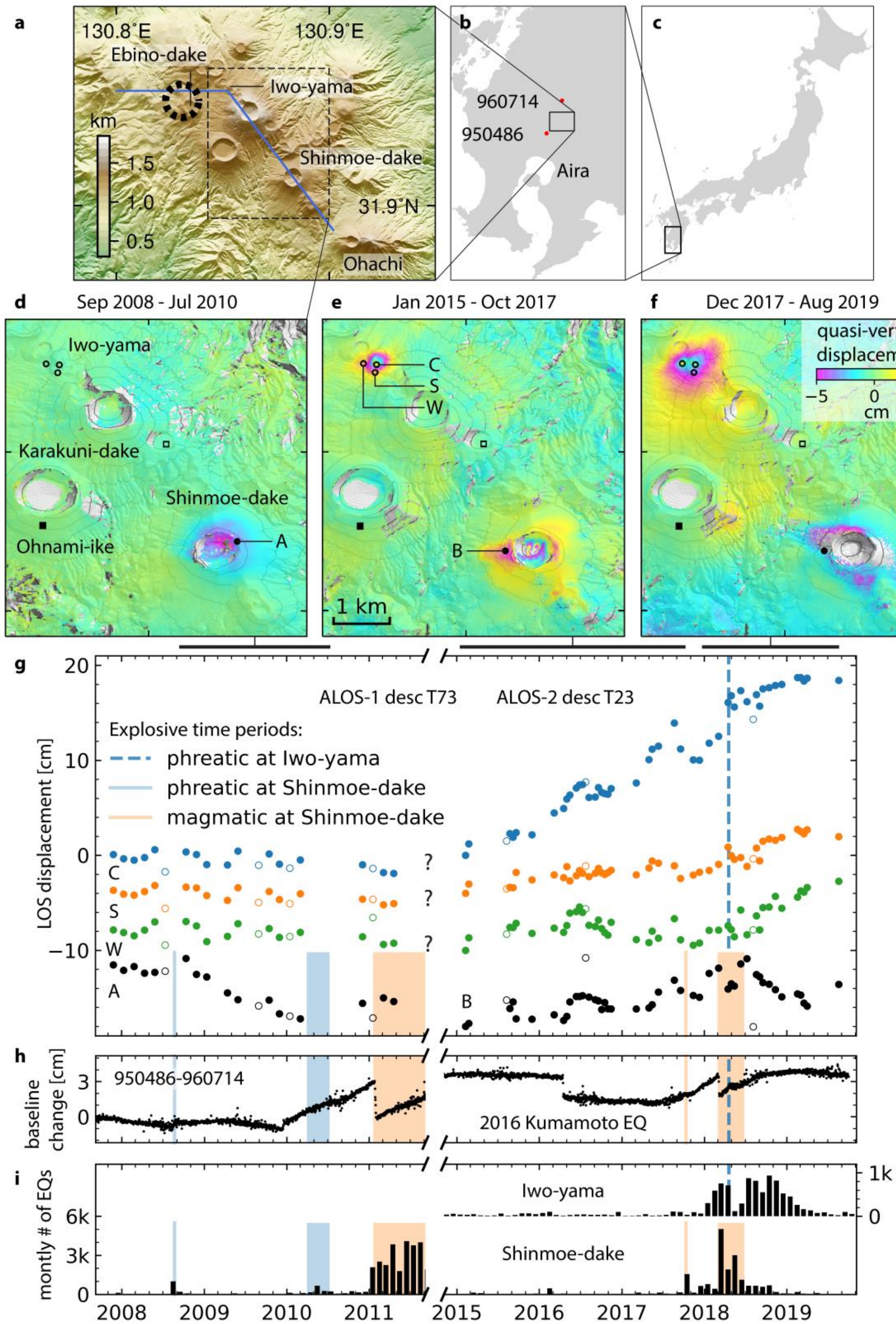

Figure 1. Geophysical observations at Kirishima during 2008-2019. (a) Geological setting. Dashed circle: horizontal location of the deep magmatic source (Nakao et al., 2013). Blue lines:

cross-section of Fig. 3c. (b-c) Location of Kirishima. Red dots: GPS sites. (d-f) Quasi-vertical displacements (d) during the 2008-2010 phreatic eruptions, (e) before and (f) after the 2017 magmatic eruption. Data are wrapped into [-5, 5) cm for display. Black squares: reference point. Contour lines in every 100 m. (g) Line-of-sight (LOS) displacement time-series at Shinmoe-dake and Iwo-yama with respect to the filled and empty black squares, respectively (shifted for display). Value increase for motion toward the satellite. Empty circles: noisy acquisitions excluded from the average velocity estimation. (h) Baseline change between two GPS stations. (i) Monthly number of earthquakes around Shinmoe-dake and Iwo-yama (JMA, 2019).

The 2011 Shinmoe-dake eruption is the first magmatic eruption in the complex since its 1716-17 eruption. Other eruptions at Shinmoe-dake in 1822, 1959 and 1991 are phreatic (Imura & Kobayashi, 1991). Iwo-yama, the youngest volcanic center, was formed in the 16th-17th century and had a phreatic eruption in 1768 (Tajima et al., 2014). Ohachi had a series of eruptions between 1880 and 1923 (GVP, 2013).

3 The 2008-2019 Activity

The unrest of Shinmoe-dake started with a substantial increase in seismicity and a rapid strain change three days before the first phreatic eruption on 22 August 2008 when a lake was present in the crater (Geshi et al., 2010; Yamazaki et al., 2020). Additional phreatic eruptions occurred from March to July 2010 (solid blue line/box in Fig. 1i). The 2011 eruption started with a phreatomagmatic eruption on 19 January and three sub-Plinian eruptions on 26-27 January, followed by stages of lava extrusion, Vulcanian and phreatomagmatic eruptions until September (Nakada et al., 2013). Shinmoe-dake had new magmatic eruptions on 11-17 October 2017 and 1 March to 27 June 2018 (solid orange line/box in Fig. 1i; GVP, 2013).

In December 2009, more than a year after the first phreatic eruption, GPS and InSAR data showed inflation over the western flank of the volcanic complex that was attributed to an inflating pressure source beneath Ebino-dake at ~10 km depth (dashed circle in Fig. 1a; Fig. 1h; Nakao et al., 2013; Miyagi et al., 2013). Rapid strain change is reported three days before this inflation (Yamazaki et al., 2020). The source deflated during the climactic phase of the 2011 Shinmoe-dake eruption and re-inflated until November 2011 (Fig. 1h; Nakao et al., 2013; Ueda et al., 2013).

About an hour and a half prior to the first sub-Plinian eruption tiltmeter and broadband seismometer recorded localized inflation near the crater suggesting a shallow pressure source (Takeo et al., 2013). In the following two weeks, this source underwent a sequence of inflation-deflation cycles during the sub-Plinian, lava extrusion and Vulcanian stages. The deformation signals, synchronized with volcanic tremors or long-period events, were attributed to the pressurization of a shallow conduit beneath the crater (Nakamichi et al., 2013; Takeo et al., 2013). Localized deflation and inflation patterns were also observed from November 2011 to May 2013 and prior to the 2017 magmatic eruption (Miyagi et al., 2014; Morishita & Kobayashi, 2018).

The unrest of Iwo-yama started with an increase in seismicity in December 2013, followed by tremors in August 2014, thermal anomalies and weak fumarolic activity since December 2015, a steam blowout event on 27 April 2017 at the crater and small phreatic eruptions on 19 and 20 April 2018 at two newly appeared vents on the southern and western side of the crater with plume heights of 100-200 m (Tajima et al., 2020). Localized pre-eruptive inflation suggests a very shallow pressure source at 150 m depth beneath the crater (Narita et al., 2020). Fumarolic activity and mud ejection continued from the southern and western vent as of December 2019 (JMA, 2019).

4 InSAR Data and Method

We use 2006-2011 ALOS-1 (ascending track 424 and descending track 73) and 2014-2019 ALOS-2 (ascending track 131 and descending track 23) L-Band stripmap SAR imagery and consider small temporal and spatial baseline interferograms (less than 1800 days and 1800 m for ALOS-1 and less than 400 days and 200 m for ALOS-2; Table S1 and Fig. S1). To form the ALOS-1 interferograms, we oversample the SAR images which are acquired in fine beam dual-polarization mode with 14 MHz bandwidth to 28 MHz, the bandwidth of fine beam single polarization mode. For the ALOS-1 and ALOS-2 interferograms, we take 8 by 10 and 4 by 10 looks in range and azimuth directions, respectively; apply a power spectral filter with a strength of 0.5 (Goldstein & Werner, 1998); remove the topographic phase using the Digital Ellipsoidal Height Model (DEHM) released by Geospatial Information Authority of Japan (GSI, 0.4 arc second, ~10 m) and unwrap the phase using the minimum cost flow method (Chen & Zebker, 2001). Ionospheric delays are not corrected.

We use the stripmap stack processor (Fattahi et al., 2017) of the ISCE software (Rosen et al., 2012) for interferogram processing and the Miami InSAR time-series software in Python (MintPy) for time series analysis (Yunjun et al., 2019). We exclude low-coherence interferograms using coherence-based network modification with a custom area of interest around Shinmoe-dake (black empty square in Fig. S2) for the average coherence calculation and thresholds of 0.7 for ALOS-1 descending track 73 and 0.8 for the others. We correct for the stratified tropospheric delay using the ERA-5 global atmospheric reanalysis model (Copernicus Climate Change Service, 2017; Jolivet et al., 2011), for topographic residuals (Fattahi &

Amelung, 2013) and for long spatial-wavelength phase components by removing linear phase ramps from all acquisitions. We use a temporal coherence threshold of 0.8 to eliminate unreliable pixels. Noisy acquisitions with residual phase root mean squares larger than the predefined cutoff (1 and 2 median absolute deviations for ALOS-1/2 dataset, respectively) are excluded during the estimation of topographic residual and average velocity (empty circles in Fig. 1g; Fig. S3).

To obtain the optimal InSAR measurement for time periods of interest (Fig. 1d-f), we apply two extra steps in addition to the routine MintPy workflow (Fig. S4-S7). First, to maximize the number of reliable pixels we exclude interferograms with acquisitions after the 2011 and 2017 eruptions, which are decorrelated by local processes inside the crater and/or by the newly deposited ash nearby. Second, to mitigate residual atmospheric turbulence we estimate the average line-of-sight (LOS) velocities for the time periods of interest and convert them to cumulative displacements instead of using the differential displacement between two acquisitions (see Fig. S8 for a comparison).

5 Results

We obtain the quasi-vertical displacements from ascending and descending data (Wright et al., 2004) during 2006-2019 to examine the deformation at the Kirishima volcanic complex and find five distinct spatial patterns: three at Shinmoe-dake and two at Iwo-yama during three different time periods (Fig. 1d-f; Fig. S9-S11). Shinmoe-dake deflated ~6 cm between the 2008-2010 phreatic eruptions (blue colors in Fig. 1d), inflated ~5 cm prior to the 2017 magmatic eruption (yellow-red colors in Fig. 1e) and has been deflating since the end of the 2018 magmatic eruption (Fig. 1f). Iwo-yama did not show any signal before 2011 (Fig. 1d) but has been inflating since at least January 2015. The deformation is localized and concentrated on the crater area during 2015-2017 (Fig. 1e), then expanded to a larger area in December 2017 (Fig.

1f), four months prior to the April 2018 phreatic eruption (dashed blue line in Fig. 1g) when new vents appeared on the southern and western side of the crater.

The LOS displacement time-series show temporal details (Fig. 1g). At Shinmoe-dake, the eastern crater rim (point A) shows no noticeable deformation prior to the 2008 phreatic eruption (solid blue line) and ~6 cm of linear LOS decrease (subsidence) between the 2008-2010 phreatic eruptions; the western crater rim (point B) shows ~4 cm of LOS increase (uplift) prior to the 2017 magmatic eruption (solid orange line) and a net ~4 cm of near-linear LOS decrease after the 2018 magmatic eruption. At Iwo-yama, the crater (point C) shows ~19 cm of near-linear LOS increase during 2014-2019 while the southern and western vents (points S and W) show no significant displacement before December 2017 but ~5 and ~7 cm of LOS increases afterward. This horizontal expansion since December 2017 coincides with the increased seismic activity (Fig. 1i). Since the end of 2018, Iwo-yama shows no noticeable displacement except for the vicinity of its western vent where linear LOS increase continues until August 2019.

Note that the relatively strong localized inflation on the western summit flank of Shinmoe-dake prior to the 2017 eruption (Fig. 1e) is likely related to a potentially partially solidified fissure from which the previous 2008-2010 eruptions occurred (Geshi et al., 2010). We do not interpret the pre-/co-/post-eruptive deformation of the 2018 Shinmoe-dake eruption as shown in the GPS baseline change (Fig. 1h) due to the overlap with the erupted ash/tephra from the 2017 eruption (Fig. 1f; Fig. S6, S7 and S12). Similar ash/tephra deposits are also observed during the 2011 eruption from phase (Fig. S13) and coherence measurement (Jung et al., 2016).

6 Modeling

We use geophysical inverse models to constrain sources of deformation at Shinmoe-dake during 2008-2010 and 2015-2017 and at Iwo-yama during 2015-2017 and 2017-2019. We assume an isotropic elastic half-space and use the vectorized finite compound dislocation models (CDM; Nikkhoo et al., 2016; see also Beauducel et al., 2020). The CDM model represents a generic ellipsoid eliminating the need to pre-specify the source geometry such as sphere or sill. For Shinmoe-dake during 2015-2017 we fixed the shape and orientation of the CDM because they can't be resolved due to the lack of near field observations (we eliminated data points inside the crater affected by local processes). For Iwo-yama during 2017-2019 we use a model with two CDMs and fix one of them with the geometry and location inferred from the previous 2015-2017 period. Although hydrothermal processes deform the ground in a thermo-poro-elastic fashion, simple elastic models are well suited to infer the source geometric features for deformation from distinct episodic unrest where poroelastic response dominates (Fournier & Chardot, 2012; Lu et al., 2002). If mechanically weak layers are present the sources will be deeper than estimated here (Manconi et al., 2007). We use a Poisson's ratio of 0.25.

We account for the elevation effect of the topography using the varying-source depth method (Williams & Wadge, 1998). To ensure that inverted pressure sources are below the free surface we assign the low-elevation data points (located in the far-field and sparsely subsampled) with height values of 1,100 m for Shinmoe-dake and of 1,300 m for Iwo-yama. The height value from GSI DEHM is converted from ellipsoid to geoid (31.2 m difference), which is not negligible considering the shallow depth.

We jointly invert the ascending and descending InSAR LOS displacement measurements using a Bayesian approach (Bagnardi & Hooper, 2018). We subsample the data using a gradient-based adaptive quadtree method (Jónsson et al., 2002) in the near field and use uniform sampling in the far-field (where the signal-to-noise ratio is low; Fig. S14). We account for the data uncertainties using structural functions (Lohman & Simons, 2005). We use uniform prior probability density functions (PDF) bounded by geologically realistic values. The inversion algorithm samples posterior PDF of source model parameters with 1,000,000 iterations. The optimal (maximum a posteriori probability) parameter value and 95% confidence intervals are shown in Table S2. All free model parameters converged well except the semi-axis along the X-axis for Shinmoe-dake during 2015-2017 and the opening of the upper CDM for Iwo-yama during 2017-2019. There are trade-offs between some parameters (see joint PDF in Fig. S15-S18) but do not affect the depth and derived volume change.

For Shinmoe-dake, the optimal solution for the 2008-2010 deflation is a slightly inclined prolate ellipsoid (Fig. 2a-e) beneath the northeastern crater section with the centroid at depth of ~620 ± 50 m below the summit (black star in Fig. 2c-d). For the 2015-2017 inflation, the optimal solution is a sphere beneath the crater center at depth of ~730 ± 210 m below the summit (black star in Fig. 2h-i). The estimated cavity volume changes for the two time periods are $-124 \pm 26 \times 10^3$ m^3 and $146 \pm 95 \times 10^3$ m^3, respectively.

For Iwo-yama, the optimal solution for the 2015-2017 inflation is a sphere with ~70 m semi-axes at depth of ~130 ± 10 m below the summit with an estimated cavity volume increase of $15 \pm 2 \times 10^3$ m^3. The optimal solution for 2017-2019 inflation is two CDMs on top of each other: one sphere with fixed parameters from the 2015-2017 period except for a free opening bounded by the 95% confidence intervals assuming a constant opening rate and one ellipsoid located at depth of ~340 ± 100 m below the summit with elongated dimension along the east-west direction. The estimated total cavity volume increase is $76 \pm 39 \times 10^3$ m^3.

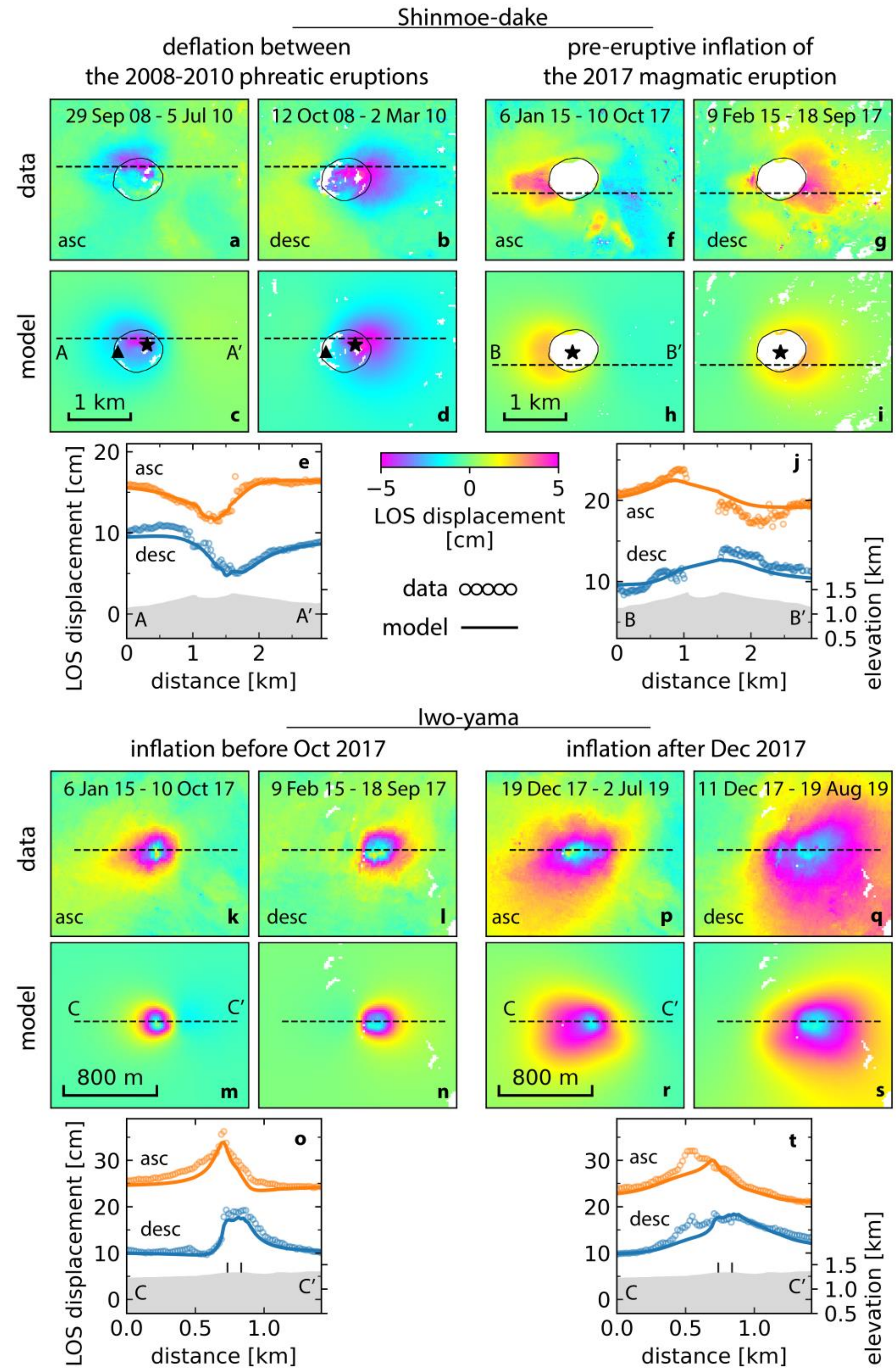

Figure 2. Geodetic modeling results at Shinmoe-dake and Iwo-yama. (a-b) Observed LOS displacement at Shinmoe-dake between the 2008-2010 eruptions from ascending and descending

orbit. (c-d) Prediction for (a-b) from the CDM. Data are wrapped into [-5, 5) cm for display. (e) Profile of observed (empty circles) and predicted (solid lines) displacement from (a-d) and the topography (gray areas). (f-j) Same as (a-e) but for Shinmoe-dake prior to the 2017 eruption. (k-o) and (p-t) Same as (a-e) but for Iwo-yama during 2015-2017 with one CDM and during 2017-2019 with two CDMs, respectively. Black circles in (a-i): Shinmoe-dake crater rim. Black triangles in (c-d): main vent of the 2008-2010 phreatic eruptions (Geshi et al., 2010). Black stars in (c-i): horizontal location of the pressure source centroid. Black vertical lines in (o and t): Iwo-yama crater.

7 Discussion

The InSAR time-series deformation provides new insights into the shallow volcanic system (within the volcanic edifice) of the central Kirishima volcanoes, in addition to a well-established deep source beneath Ebino-dake at ~10 km depth below the surface.

7.1 Shinmoe-dake: Hydrothermal origin of the 2008-2010 deflation

The deflation between the 2008-2010 phreatic eruptions is of hydrothermal origin, as most of the erupted material before March 2010 is hydrothermally altered (<1 vol% of juvenile material; Suzuki et al., 2013). This is consistent with geoelectrical-detected widespread shallow low-resistivity, water-saturated porous layers (e.g. Aizawa et al., 2014). Furthermore, most of the deflation occurred before December 2009 when the deep source began to inflate (point A in Fig. 1g).

The prolate geometry from geodetic modeling could indicate the depressurization of a former magmatic conduit. The estimated cavity volume decrease ($124 \pm 26 \times 10^3$ m^3) is similar to the volume of erupted tephra (120×10^3 m^3; Geshi et al., 2010) from the August 2008 eruption. No noticeable co-eruptive deformation is observed from InSAR (point A in Fig. 1g). A possible mechanism is that the August 2008 eruption unsealed the system and emptied the reservoir, which was immediately refilled by hydrothermal fluids; these fluids were released via steam emission (JMA, 2019) during 2008-2010, resulting in surface subsidence.

7.2 Shinmoe-dake: Replacement of hydrothermal system by magmatic body

The 2015-2017 inflation prior to a magmatic eruption was almost certainly magmatic, as indicated by the elevated SO_2 emission higher than the background level since 2011 (JMA, 2019). The inferred depth of 730 m is very similar to 2008-2010 (overlapping PDFs in Fig. 3a). A similar source depth was also inferred for the Vulcanian stage of the 2011 magmatic eruption (Takeo et al., 2013) and for November 2011 to May 2013 magma extrusion period (Miyagi et al., 2014). These depths suggest that the deflation/inflation during the above four periods are from the same source. Together, the similar geodetic source depths, the appearance and dominance of SO_2 fluxes and juvenile materials from ash samples suggest that part of the porous rock mass that acted as a hydrothermal source in 2008-2010 was replaced by a magmatic body during the 2011 eruption and stayed as magmatic since then. This is similar to the 2014-2015 phreatic-magmatic transitions in Turrialba volcano inferred from gas emission data (de Moor et al., 2016) but at a much shallower level and transited only once.

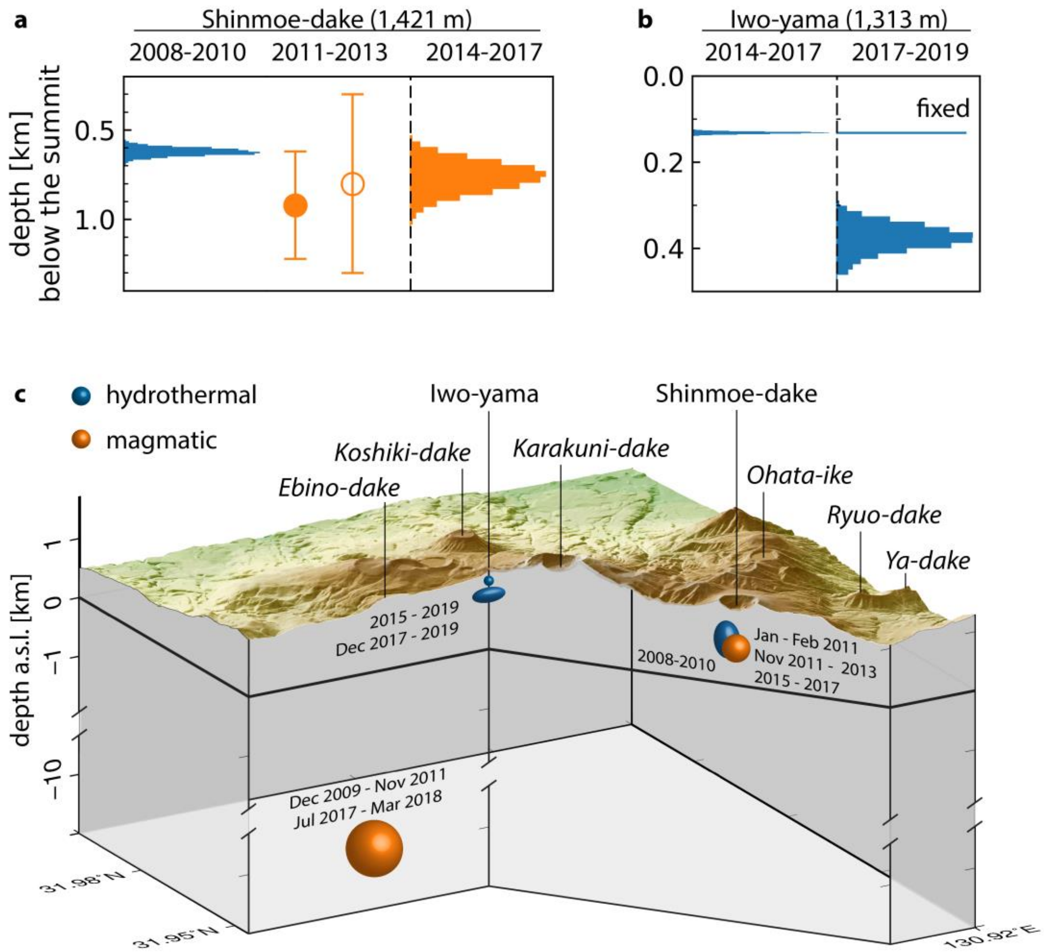

Figure 3. Conceptual model of the magmatic and hydrothermal pressure sources at the Kirishima volcanic complex. (a) Marginal posterior density distributions of depths of pressure source beneath Shinmoe-dake. From left to right: 1) deflation between the 2008-2010 phreatic eruptions, 2) inflation-deflation cycles (filled error bar) during the Vulcanian stage in February 2011 (Takeo et al., 2013), 3) deflation (empty error bar) during the 2011-2013 lava extrusion stage (Miyagi et al., 2014) and 4) inflation before the 2017 magmatic eruption. (b) Same as (a) but beneath Iwo-yama for inflation before and after December 2017, respectively. (c) Conceptual model of the plumbing system. The 2008-2010 Shinmoe-dake source has the inferred dimension. The size of the other sources reflects the ratio of their volume changes and the 2008-2010

Shinmoe-dake volume change, except for the deep magmatic source. The topography is vertically exaggerated by 25%.

7.3 Iwo-yama: Triple-source hydrothermal system

The expanded inflation at Iwo-yama since December 2017 cannot be explained by the single source at 130 m depth (very well constrained with a 95% confidence interval of <10 m due to the shallow depth and coherent near-/far-field observation). Geodetic modeling suggests an extra east-west oriented lay-down cigar-shaped source further down at depth of 340 m (Fig. 2p-t and 3b) with two sources on top of each other at very shallow depths prior to the eruption. Both sources are hydrothermal as evident from the strong fumarolic activity, steam emissions, and ejection of mud and hot water since 2014 (JMA, 2019).

The upper source at 130 m depth (1180 m a.s.l.) has been inflating since at least January 2015 (point C in Fig. 1g). There is a minor peak location change during 2016-2018 around the Iwo-yama crater (Narita et al., 2020). Geochemical analysis in 2016 shows that the water is meteoric (Tajima et al., 2020), suggesting the upward migration of magmatic fluid is not the primary direct driver. Geoelectric surveys have resolved a low-resistivity zone at 200-700 m depth (Tsukamoto et al., 2018), which is below the upper source thus can not serve as caprocks for hydrothermal sealing to support persistent overpressure. The fumarolic temperature has continuously been around or above 96 ℃ (Tajima et al., 2020), which is the water boiling point temperature at 1180 m a.s.l. Thus, we conclude that the liquid-gas two-phase boiling of meteoric water is the primary driver of the persistent localized inflation around the Iwo-yama crater.

The lower source at 340 m depth hosts the southern and western vent and is responsible for the April 2018 eruption. Considering 1) the mix of meteoric and magmatic water from the geochemical analysis in 2018 before the eruption and 2) the observation of days of fluid upwelling just before the 2017 blowout and 2018 eruption (Tajima et al., 2020), we interpret the expanded inflation is driven by the bottom-up pressurization from the upward migration of magmatic fluid at depth.

Residuals of geodetic modeling show a localized uplift at the western vent after December 2017 (Fig. S19 and the difference between solid lines and empty circles in Fig. 2t). The small spatial scale (~150 m in diameter) and the exact same location from ascending and descending orbits suggest the corresponding pressure source is even shallower than the one at 130 m depth. In total, Iwo-yama hosts a complex hydrothermal system with three tiny reservoirs at very shallow depths.

7.4 Conceptual model of the Kirishima plumbing system

The magmatic and hydrothermal plumbing system of the Kirishima volcanic complex is summarized in Fig. 3c. A deep (~10 km below the surface) magmatic source beneath Ebino-dake inflated between December 2009 and the 2011 eruption (Fig. S13) and inflated again between the 2017 and 2018 eruption (Fig. 1h). The shallow source beneath Shinmoe-dake (~700 m below the summit) was hydrothermally evacuating gas and steam between the 2008-2010 phreatic eruptions, then turned magmatic during the 2011 eruption and has been accumulating magma since at least January 2015, feeding the 2017 and 2018 magmatic eruptions. The very shallow hydrothermal reservoir beneath Iwo-yama (130 m below the summit) has been boiling since at least January 2015. In December 2017 another slightly deeper hydrothermal reservoir (340 m below the summit) started accumulating magmatic fluid, feeding the April 2018 phreatic eruption. The western vent of Iwo-yama was still inflating as of August 2019.

8 Conclusions

We derived the surface deformation history of the Kirishima volcanic complex during 2006-2011 and 2014-2019 using InSAR time series analysis. Built upon the routine workflow, we demonstrated that excluding interferograms after destructive eruptions and using average velocity could increase the spatial coverage of near-field observation and further beat down the residual tropospheric turbulence after tropospheric correction, to improve the displacement estimate for time periods of interest.

Combining geodetic and petrologic data, we identified the hydrothermal reservoir beneath Shinmoe-dake subsiding after the August 2008 eruption, much earlier than the previously thought precursory magmatic inflation since December 2009. The compilation of multiple geodetic studies suggests this hydrothermal reservoir is replaced by a magmatic body during the 2011 eruption. At Iwo-yama, the deformation time-series reveals a precursory horizontal expansion for the 2018 eruption. We propose a hydrothermal system with three tiny reservoirs beneath Iwo-yama at very shallow levels to explain the observed deformation. Combining geodetic, geoelectric and geochemical data, we conclude that the deformation is driven by liquid-gas two-phase boiling of meteoric water at the upper reservoir and bottom-up pressurization from upward migration of magmatic water at the lower reservoir. The study highlights the imaging potential of InSAR time-series for complex hydrothermal systems and the importance of multidiscipline data for the understanding of volcanic processes.

Data and Code Availability

The InSAR displacement products and geodetic modeling results are available on Zenodo (https://doi.org/10.5281/zenodo.4495798, https://doi.org/10.5281/zenodo.4499238 and https://doi.org/10.5281/zenodo.4499208). Figures are prepared using GMT (Wessel et al., 2013) and Matplotlib (Hunter, 2007) in Jupyter Notebook available on Zenodo (https://doi.org/10.5281/zenodo.4532177).

Acknowledgments

The ALOS-1/2 data are shared among the PALSAR Interferometry Consortium to Study our Evolving Land surface (PIXEL) and provided by JAXA under contract with the University of Tokyo. The ownership of ALOS-1/2 SAR data belongs to JAXA and the Ministry of Economy Trade and Industry. We thank GSI for the DEHM and GPS data, the Japan Meteorological Agency (JMA) for the earthquake data. We thank Jamie Farquharson, Heresh Fattahi, Mehdi Nikkhoo and Bhuvan Varugu for discussions. This work was supported by NASA Headquarters under the Earth and Space Science Fellowship program (Grant No. NNX15AN13H) and National Science Foundation's Geophysics program (Grant No. EAR1345129).

References

Aizawa, K., et al. (2014), Three-dimensional resistivity structure and magma plumbing system of the Kirishima Volcanoes as inferred from broadband magnetotelluric data, *Journal of Geophysical Research: Solid Earth*, *119*(1), 198-215, doi:10.1002/2013jb010682.

Bagnardi, M., and A. Hooper (2018), Inversion of Surface Deformation Data for Rapid Estimates of Source Parameters and Uncertainties: A Bayesian Approach, *Geochemistry, Geophysics, Geosystems*, *19*, doi:10.1029/2018GC007585.

Battaglia, M., C. Troise, F. Obrizzo, F. Pingue, and G. De Natale (2006), Evidence for fluid migration as the source of deformation at Campi Flegrei caldera (Italy), *Geophysical Research Letters*, *33*(1), doi:10.1029/2005GL024904.

Beauducel, F., A. Peltier, A. Villié, and W. Suryanto (2020), Mechanical Imaging of a Volcano Plumbing System From GNSS Unsupervised Modeling, *Geophysical Research Letters*, *47*(17), e2020GL089419, doi:10.1029/2020GL089419.

Brothelande, E., F. Amelung, Z. Yunjun, and S. Wdowinski (2018), Geodetic evidence for interconnectivity between Aira and Kirishima magmatic systems, Japan, *Scientific Reports*, *8*(1), 9811, doi:10.1038/s41598-018-28026-4.

Chapman N., Apted M., Beavan J., Berryman K., Cloos M., Connor C. et al. (2009), Development of Methodologies for the Identification of Volcanic and Tectonic Hazards to Potential HLW Repository Sites in Japan: the Kyushu Case Study, in *NUMO-TR-09-02*, edited, Nuclear Waste Management Organization of Japan.

Chen, C. W., and H. A. Zebker (2001), Two-dimensional phase unwrapping with use of statistical models for cost functions in nonlinear optimization, *JOSA A*, *18*(2), 338-351, doi:10.1364/JOSAA.18.000338.

Christiansen, R. L., D. W. Peterson, P. Lipman, and D. Mullineaux (1981), Chronology of the 1980 eruptive activity, *US Geol. Surv. Prof. Pap*, *1250*, 17-30, doi:10.3133/pp1250.

Copernicus Climate Change Service (2017): ERA5: Fifth generation of ECMWF atmospheric reanalyses of the global climate. *Copernicus Climate Change Service Climate Data Store*, date of access: 3 June 2019. https://cds.climate.copernicus.eu/cdsapp#!/home

de Moor, J. M., et al. (2016), Turmoil at Turrialba Volcano (Costa Rica): Degassing and eruptive processes inferred from high-frequency gas monitoring, *Journal of Geophysical Research: Solid Earth*, *121*(8), 5761-5775, doi:10.1002/2016jb013150.

Fattahi, H., and F. Amelung (2013), DEM Error Correction in InSAR Time Series, *Geoscience and Remote Sensing, IEEE Transactions on*, *51*(7), 4249-4259, doi:10.1109/TGRS.2012.2227761.

Fattahi, H., M. Simons, and P. Agram (2017), InSAR Time-Series Estimation of the Ionospheric Phase Delay: An Extension of the Split Range-Spectrum Technique, *IEEE Transactions on Geoscience and Remote Sensing*, *55*(10), 5984-5996, doi:10.1109/TGRS.2017.2718566.

Fournier, N., and L. Chardot (2012), Understanding volcano hydrothermal unrest from geodetic observations: Insights from numerical modeling and application to White Island volcano, New Zealand, *Journal of Geophysical Research: Solid Earth*, *117*(B11), doi:10.1029/2012jb009469.

Germanovich, L. N., and R. P. Lowell (1995), The mechanism of phreatic eruptions, *Journal of Geophysical Research: Solid Earth*, *100*(B5), 8417-8434, doi:10.1029/94jb03096.

Geshi, N., S. Takarada, M. Tsutsui, T. Mori, and T. Kobayashi (2010), Products of the August 22, 2008 eruption of Shinmoedake Volcano, Kirishima Volcanic Group, Japan, *BULLETIN OF THE VOLCANOLOGICAL SOCIETY OF JAPAN*, *55*(1), 53-64, doi:10.18940/kazan.55.1_53 (in Japanese).

Goldstein, R. M., and C. L. Werner (1998), Radar interferogram filtering for geophysical applications, *Geophysical Research Letters*, *25*(21), 4035-4038, doi:10.1029/1998GL900033.

GVP (Global Volcanism Program) (2013). Kirishimayama (282090) *in* Volcanoes of the World, v. 4.9.0 (04 Jun 2020). Venzke, E (ed.). Smithsonian Institution. Downloaded 17 Aug 2020 (https://volcano.si.edu/volcano.cfm?vn=282090). https://doi.org/10.5479/si.GVP.VOTW4-2013

Hamling, I. J., C. A. Williams, and S. Hreinsdóttir (2016), Depressurization of a hydrothermal system following the August and November 2012 Te Maari eruptions of Tongariro, New Zealand, *Geophysical Research Letters*, *43*(1), 168-175, doi:10.1002/2015gl067264.

Himematsu, Y., T. Ozawa, and Y. Aoki (2020), Coeruptive and posteruptive crustal deformation associated with the 2018 Kusatsu-Shirane phreatic eruption based on PALSAR-2 time series analysis, *Earth Planet Sp*, *72*(1), 116, doi:10.1186/s40623-020-01247-6.

Hunter, J. D. (2007), Matplotlib: A 2D Graphics Environment, *Computing in Science & Engineering*, *9*(3), 90-95, doi:10.1109/MCSE.2007.55.

Imura, R., and T. Kobayashi (1991), Eruptions of Shinmoedake volcano, Kirishima volcano group, in the last 300 years, *Bull. Volcanol. Soc. Jpn*, *36*, 135-148, doi:10.18940/kazan.36.2_135 (in Japanese).

JMA (Japan Meteorological Agency) (2019), 2007-2019 Annual Reports of Volcanic Activity at Kirishima, *Volcanic Activity Explanation Material*, http://www.data.jma.go.jp/svd/vois/data/

tokyo/STOCK/monthly_v-act_doc/monthly_vact_vol.php?id=505 (accessed on 29 Jan 2020; in Japanese).

Jolivet, R., R. Grandin, C. Lasserre, M. P. Doin, and G. Peltzer (2011), Systematic InSAR tropospheric phase delay corrections from global meteorological reanalysis data, *Geophysical Research Letters*, *38*(17), L17311, doi:10.1029/2011GL048757.

Jónsson, S., H. Zebker, P. Segall, and F. Amelung (2002), Fault Slip Distribution of the 1999 Mw 7.1 Hector Mine, California, Earthquake, Estimated from Satellite Radar and GPS Measurements, *Bulletin of the Seismological Society of America*, *92*(4), 1377-1389, doi:10.1785/0120000922.

Jung, J., D. j. Kim, M. Lavalle, and S. H. Yun (2016), Coherent Change Detection Using InSAR Temporal Decorrelation Model: A Case Study for Volcanic Ash Detection, *IEEE Transactions on Geoscience and Remote Sensing*, *54*(10), 5765-5775, doi:10.1109/TGRS.2016.2572166.

Kobayashi, T., Y. Morishita, and H. Munekane (2018), First detection of precursory ground inflation of a small phreatic eruption by InSAR, *Earth and Planetary Science Letters*, *491*, 244-254, doi:10.1016/j.epsl.2018.03.041.

Lohman, R. B., and M. Simons (2005), Some thoughts on the use of InSAR data to constrain models of surface deformation: Noise structure and data downsampling, *Geochemistry, Geophysics, Geosystems*, *6*(1), doi:10.1029/2004GC000841.

Lu, Z., T. Masterlark, J. Power, D. Dzurisin, and C. Wicks (2002), Subsidence at Kiska Volcano, Western Aleutians, detected by satellite radar interferometry, *Geophysical Research Letters*, *29*(18), 2-1-2-4, doi:10.1029/2002gl014948.

Lundgren, P., S. Usai, E. Sansosti, R. Lanari, M. Tesauro, G. Fornaro, and P. Berardino (2001), Modeling surface deformation observed with synthetic aperture radar interferometry at Campi Flegrei caldera, *Journal of Geophysical Research: Solid Earth*, *106*(B9), 19355-19366, doi:10.1029/2001jb000194.

Manconi, A., T. R. Walter, and F. Amelung (2007), Effects of mechanical layering on volcano deformation, *Geophysical Journal International*, *170*(2), 952-958, doi:10.1111/j.1365-246X.2007.03449.x.

Miyagi, Y., T. Ozawa, and Y. Kohno (2013), Crustal Deformation Associated with the 2011 Eruption of Shinmoe-dake in Kirishima Volcano Group, Southwestern Japan, Detected by DInSAR and GPS Measurements, *BULLETIN OF THE VOLCANOLOGICAL SOCIETY OF JAPAN*, *58*(2), 341-351, doi:10.18940/kazan.58.2_341 (in Japanese).

Miyagi, Y., T. Ozawa, T. Kozono, and M. Shimada (2014), Long-term lava extrusion after the 2011 Shinmoe-dake eruption detected by DInSAR observations, *Geophysical Research Letters*, *41*(16), 5855-5860, doi:10.1002/2014GL060829.

Morishita, Y., and T. Kobayashi (2018), Ground Surface Displacement of Kirishima Volcano Group Detected by ALOS-2 InSAR Time Series Analysis and Effect of Atmospheric Noise Reduction, *Journal of the Geodetic Society of Japan*, *64*, 28-38, doi:10.11366/sokuchi.64.28 (in Japanese).

Muffler, L. J. P., D. E. White, and A. H. Truesdell (1971), Hydrothermal Explosion Craters in Yellowstone National Park, *GSA Bulletin*, *82*(3), 723-740, doi:10.1130/0016-7606(1971)82[723:Heciyn]2.0.Co;2.

Nakaboh, M., H. Ono, M. Sako, Y. Sudo, T. Hashimoto, and A. W. Hurst (2003), Continuing deflation by fumaroles at Kuju Volcano, Japan, *Geophysical Research Letters*, *30*(7), doi:10.1029/2002gl016047.

Nakada, S., M. Nagai, T. Kaneko, Y. Suzuki, and F. Maeno (2013), The outline of the 2011 eruption at Shinmoe-dake (Kirishima), Japan, *Earth, Planets, and Space*, *65*, 475-488, doi:10.5047/eps.2013.03.016.

Nakamichi, H., Y. Yamanaka, T. Terakawa, S. Horikawa, T. Okuda, and F. Yamazaki (2013), Continuous long-term array analysis of seismic records observed during the 2011 Shinmoedake eruption activity of Kirishima volcano, southwest Japan, *Earth Planets Space*, *65*(6), 551-562, doi:10.5047/eps.2013.03.002.

Nakao, S., Y. Morita, H. Yakiwara, J. Oikawa, H. Ueda, H. Takahashi, Y. Ohta, T. Matsushima, and M. Iguchi (2013), Volume change of the magma reservoir relating to the 2011 Kirishima Shinmoe-dake eruption—Charging, discharging and recharging process inferred from GPS measurements, *Earth Planets Space*, *65*(6), 505-515, doi:10.5047/eps.2013.05.017.

Narita, S., and M. Murakami (2018), Shallow hydrothermal reservoir inferred from post-eruptive deflation at Ontake Volcano as revealed by PALSAR-2 InSAR, *Earth Planet Sp*, *70*(1), 191, doi:10.1186/s40623-018-0966-6.

Narita, S., T. Ozawa, Y. Aoki, M. Shimada, M. Furuya, Y. Takada, and M. Murakami (2020), Precursory ground deformation of the 2018 phreatic eruption on Iwo-Yama volcano, revealed by four-dimensional joint analysis of airborne and spaceborne InSAR, *Earth Planet Sp*, *72*(1), 145, doi:10.1186/s40623-020-01280-5.

Newhall, C. G., and R. Punongbayan (1996), *Fire and mud: eruptions and lahars of Mount Pinatubo, Philippines*, Philippine Institute of Volcanology and Seismology Quezon City.

Nikkhoo, M., T. R. Walter, P. R. Lundgren, and P. Prats-Iraola (2016), Compound dislocation models (CDMs) for volcano deformation analyses, *Geophysical Journal International*, *208*(2), 877-894, doi:10.1093/gji/ggw427.

Ohba, T., K. Nogami, and J.-i. Hirabayashi (1997), Hydrothermal System of the Kirishima Volcanic Area Inferred from the Chemical and Isotopic Composition of Spring Waters and Fumarolic Gases, *BULLETIN OF THE VOLCANOLOGICAL SOCIETY OF JAPAN*, *42*(1), 1-15, doi:10.18940/kazan.42.1_1.

Rosen, P. A., E. Gurrola, G. F. Sacco, and H. Zebker (2012), The InSAR scientific computing environment, paper presented at EUSAR 2012, 23-26 April 2012.

Stix, J., and J. M. de Moor (2018), Understanding and forecasting phreatic eruptions driven by magmatic degassing, *Earth Planet Sp*, *70*(1), 83, doi:10.1186/s40623-018-0855-z.

Suzuki, Y., M. Nagai, F. Maeno, A. Yasuda, N. Hokanishi, T. Shimano, M. Ichihara, T. Kaneko, and S. Nakada (2013), Precursory activity and evolution of the 2011 eruption of Shinmoe-dake in Kirishima volcano-insights from ash samples, *Earth, Planets, and Space*, *65*, 591-607, doi:10.5047/eps.2013.02.004.

Tajima, Y., Y. Matsuo, T. Shoji, and T. Kobayashi (2014), Eruptive History of Ebinokogen Volcanic Area of Kirishima Volcanoes for the Past 15,000 Years in Kyushu, Japan, *BULLETIN OF THE VOLCANOLOGICAL SOCIETY OF JAPAN*, *59*(2), 55-75, doi:10.18940/kazan.59.2_55 (in Japanese).

Tajima, Y., S. Nakada, F. Maeno, T. Huruzono, M. Takahashi, A. Inamura, T. Matsushima, M. Nagai, and J. Funasaki (2020), Shallow Magmatic Hydrothermal Eruption in April 2018 on Ebinokogen Ioyama Volcano in Kirishima Volcano Group, Kyushu, Japan, *Geosciences*, *10*(5), 183, doi:10.3390/geosciences10050183.

Takeo, M., Y. Maehara, M. Ichihara, T. Ohminato, R. Kamata, and J. Oikawa (2013), Ground deformation cycles in a magma-effusive stage, and sub-Plinian and Vulcanian eruptions at Kirishima volcanoes, Japan, *Journal of Geophysical Research: Solid Earth*, *118*(9), 4758-4773, doi:10.1002/jgrb.50278.

Tsukamoto, K., K. Aizawa, K. Chiba, W. Kanda, M. Uyeshima, T. Koyama, M. Utsugi, K. Seki, and T. Kishita (2018), Three-Dimensional Resistivity Structure of Iwo-Yama Volcano, Kirishima Volcanic Complex, Japan: Relationship to Shallow Seismicity, Surface Uplift, and a Small Phreatic Eruption, *Geophysical Research Letters*, *45*(23), 12,821-812,828, doi:10.1029/2018gl080202.

Ueda, H., T. Kozono, E. Fujita, Y. Kohno, M. Nagai, Y. Miyagi, and T. Tanada (2013), Crustal deformation associated with the 2011 Shinmoe-dake eruption as observed by tiltmeters and GPS, *Earth Planets Space*, *65*(6), 517-525, doi:10.5047/eps.2013.03.001.

Wallace, L. M., S. Ellis, K. Miyao, S. Miura, J. Beavan, and J. Goto (2009), Enigmatic, highly active left-lateral shear zone in southwest Japan explained by aseismic ridge collision, *Geology*, *37*(2), 143-146, doi:10.1130/G25221A.1.

Wessel, P., W. H. Smith, R. Scharroo, J. Luis, and F. Wobbe (2013), Generic mapping tools: improved version released, *Eos, Transactions American Geophysical Union*, *94*(45), 409-410, doi:10.1002/2013EO450001.

Williams, C. A., and G. Wadge (1998), The effects of topography on magma chamber deformation models: Application to Mt. Etna and radar interferometry, *Geophysical Research Letters*, *25*(10), 1549-1552, doi:10.1029/98gl01136.

Wright, T. J., B. E. Parsons, and Z. Lu (2004), Toward mapping surface deformation in three dimensions using InSAR, *Geophysical Research Letters*, *31*(1), L01607, doi:10.1029/2003GL018827.

Yamazaki, K. i., Y. Yamashita, and S. Komatsu (2020), Vault-housed extensometers recorded a rapid initial pulse before precursory magma reservoir inflation related to the 2011 eruption of Shinmoe-dake, Japan, *Earth Planet Sp*, *72*(1), 83, doi:10.1186/s40623-020-01211-4.

Yunjun, Z., H. Fattahi, and F. Amelung (2019), Small baseline InSAR time series analysis: Unwrapping error correction and noise reduction, *Computers & Geosciences*, *133*, 104331, doi:10.1016/j.cageo.2019.104331.